


RESEARCH

Open Access



Integrated high-throughput small RNA and transcriptome sequencing unveil the shape-dependent toxicity of nano-alumina in rat astrocytes

Yuanyuan Chen^{1†}, Li Dong^{1†}, Fuchang Deng¹, Yaqiang Cao^{1,2}, Yuanzheng Fu¹, Mu Zhu¹, Guangqiu Qin³, Dayna Schultz⁴, Kamran Shekh⁵ and Song Tang^{1,2*} 

Abstract

Background: The large-scale applications of alumina nanoparticles (Al_2O_3 -NPs), one of the most important NPs in the global market, are causing severe damages to the environment and human health. Our previous research has revealed a critical role of nanoparticle morphology (e.g., flake and rod) in determining the toxic potencies of Al_2O_3 -NPs, where nanorods demonstrated a significantly stronger toxic response than that of nanoflakes. However, their underlying mechanisms have not been completely elucidated yet. In the present study, we evaluated and compared the potential toxicological mechanisms of two shapes of γ - Al_2O_3 -NPs (flake versus rod) by measuring miRNA and mRNA profiles of astrocytes in rat cerebral cortex, ex vivo.

Results: A total of 269 mRNAs and 122 miRNAs, 180 mRNAs and 116 miRNAs were differentially expressed after nanoflakes or nanorods exposure, respectively. Among them, 55 miRNAs (e.g., miR-760-5p, miR-326-3p, and miR-35) and 105 mRNAs (e.g., *Kdm4d*, *Wdr62*, and *Rps6*) showed the same trend between the two shapes. These miRNAs and mRNAs were mainly involved in apoptosis, inflammatory pathways (e.g., NF-kappa B), carcinogenic pathways (e.g., MAPK, p53, Notch, Rap1, and Ras), and cellular lipid metabolisms (e.g., glycerolipid metabolism, sphingolipid, and ether lipid metabolism). However, the remaining miRNAs and mRNAs either showed an opposite trend or only changed by a particular shape. Nanorods could specifically alter the changes of PI3K/Akt, AMPK and TNF pathways, cell cycle, and cellular senescence, while nanoflakes caused the changes of Toll and Imd signaling pathways.

Conclusions: Combined with previous research results, we further revealed the potential biomolecular mechanisms leading to the stronger toxicity of nanorods than that of nanoflakes, and multi-omics is a powerful approach to elucidate morphology-related mode of actions.

Keywords: Nanoparticles, Morphology, High-throughput sequencing, MicroRNAs, Transcriptome, Pathway analysis

Introduction

With the rapidly increasing applications of nanoparticles (NPs), the annual output of NPs has sharply grown from 2300 tons in 2008 to nearly 58,000 tons in 2020 [1]. Alumina nanoparticles (Al_2O_3 -NPs), one of the most important commercial NP productions in the global market, are widely used in pharmaceutical products, biomaterials, and high-energy systems [2, 3]. Unfortunately, the

*Correspondence: dongli@nieh.chinacdc.cn; tangsong@nieh.chinacdc.cn

[†]Yuanyuan Chen and Li Dong contributed equally to this work

¹ China CDC Key Laboratory of Environment and Population Health, National Institute of Environmental Health, Chinese Center for Disease Control and Prevention, No. 7 Panjiayuan Nanli, Chaoyang District, Beijing 100021, China

Full list of author information is available at the end of the article

tremendous development of nanotechnology and excessive application of Al_2O_3 -NPs has inevitably brought its increased burden on the environment and human health [4]. Although earlier epidemiological and toxicological studies have demonstrated that Al_2O_3 -NPs exposure could lead to Alzheimer's disease and other neurodegenerative disorders [5, 6], which could be linked to oxidative stress, inflammation, genotoxicity, and cell death [7–10], their underlying toxicological mechanisms still remain to be understood.

Many factors significantly affect the toxicity of NPs, including their physical and chemical properties (e.g., size, shape, and structure characteristics), concentrations, incubation time, and receptor cell types [8]. Previous reports have mostly focused on Al_2O_3 -NPs toxicities induced by particles of various sizes or structures [11, 12]; however, the toxicity induced by different particle shapes has been rarely reported. For instance, it was demonstrated that four different shapes of hydroxyapatite NPs could increase reactive oxygen (ROS) production, alkaline phosphatase activity and the concentration of calcium, and decrease the mitochondrial membrane potential and lysosome integrity, and the toxicity potential of four shapes were ranked as follows: plate > sphere > needle > rod [13]. In our previous study, the toxicities of $\gamma\text{-Al}_2\text{O}_3$ -NPs of two different shapes (flake versus rod) and their effects on metabolic profiles were compared in the astrocytes (ASTs) of rat cerebral cortex, *ex vivo* [14]. Significantly stronger cytotoxicity and apoptosis were observed for nanorods than for nanoflakes, which were associated with significantly greater ROS accumulation, apoptosis, inflammation induction, and metabolic responses. However, the underlying mechanisms for the shape-induced nanotoxicity, especially at the microRNA (miRNA) and transcriptional (mRNA) expression levels, were not completely understood in the study.

Omics (e.g., epigenomics and transcriptomics) have been recognized as a comprehensive and efficient approach to identify new biomarkers and to elucidate specific mechanisms driving toxicological effects induced by nano-alumina [15]. For example, mRNA profiling has been used in Al_2O_3 -NP-exposed human bronchial epithelial (HBE) cells, showing differentially expressed genes encoding proteins essential for mitochondrial function, such as oxidative phosphorylation [4]. The toxicities of various surface modified Al_2O_3 -NPs (pristine, hydrophilic or lipophilic) to *Caenorhabditis elegans* (*C. elegans*) have been found to differ, with lipophilic NPs being the most toxic modification [16]. The lipophilic Al_2O_3 -NPs could significantly induce excessive ROS production, destroy the redox balance, and lead to apoptosis [17]. Moreover, transcriptomic analysis further showed that miR-297 was

significantly up-regulated in HBE cells, inducing pulmonary inflammation via the Notch pathway [17]. Furthermore, Al_2O_3 -NPs could cause an increase in expressions of miR-395, miR-397, miR-398, and miR-399 in tobacco seedlings [18]. However, to date, the integrated application of a variety of genetically related omics approaches to systematically evaluate the impact of different shapes of Al_2O_3 -NPs exposure is relatively scarce.

As an extension of our previous work [14], in the present study, we exposed rat primary ASTs to $\gamma\text{-Al}_2\text{O}_3$ -NPs of two distinct shapes (flake versus rod) at a dose of 125 $\mu\text{g/mL}$ for 72 h with the aims to: (1) comprehensively characterize the differentially expressed miRNAs and mRNAs through high-throughput small RNA and transcriptome sequencings; (2) identify the miRNAs and mRNAs specifically responding to nanoflakes or nanorods; (3) explore the interactions between miRNA and mRNA responding to the distinct toxicities of nanoflakes and nanorods, for a further understanding of their underlying mechanisms or pathways.

Materials and methods

Nanoparticles preparation and sample collection

$\gamma\text{-Al}_2\text{O}_3$ -NPs were successfully synthesized and fully characterized (e.g., particle size and shape) as reported in our previous study [14]. Rat primary ASTs were extracted from the cortex of neonatal 24-h-old Wistar rats (purchased from the Chinese Experimental Animal Center of Military Medical Science Academy, Beijing, China) as previously described [14]. Before the experiment, two differently shaped (flake or rod) $\gamma\text{-Al}_2\text{O}_3$ -NPs were dispersed in DMEM/F12 medium (HyClone, Beijing, China), sonicated and shaken for 30 min at 20 °C. Rat ASTs were then exposed to nanoflakes and nanorods at the concentration of 125 $\mu\text{g/mL}$ for 72 h with significant cytotoxicity observed. The same volume of culture medium without $\gamma\text{-Al}_2\text{O}_3$ -NPs was used as a control. Three parallel controls were set in each group. After exposure, cells were washed in cold phosphate buffered saline (PBS) for three times and total RNA was isolated using Trizol (Invitrogen, Carlsbad, CA, USA) [19].

Total RNA extraction

After exposure, total RNA was extracted from the cells using Trizol (Invitrogen, Carlsbad, CA, USA) according to the supplier's instructions. Briefly, samples were centrifuged for 5 min with 12,000 $\times g$ at 4 °C, and supernatants were transferred into a new RNAase-free Eppendorf tube with 0.3 mL chloroform/isoamyl alcohol (24:1). The mix was shaken for 15 s, and then centrifuged at 12,000 $\times g$ for 10 min at 4 °C. After centrifugation, RNA containing the upper aqueous phase was transferred into a new RNAase-free tube with equal volume of supernatant of isopropyl

alcohol, then centrifuged at $12,000\times$ rpm for 20 min at 4 °C. After discarding the supernatant, RNA pellets were washed twice with 1 mL of 75% ethanol. The mix was then centrifuged at $12,000\times$ rpm for 3 min at 4 °C to collect residual ethanol, and then the pellet was allowed to air dry for 10 min. Finally, 25 μ L of diethylpyrocarbonate-treated water was added to dissolve the RNA. Total RNA was qualified and quantified using a NanoDrop ND-2000 and Agilent 2100 bioanalyzer (Thermo Fisher Scientific, MA, USA).

miRNA library preparation and sequencing

A library of miRNA was prepared with 1 μ g total RNA for each sample. Total RNA was purified by electrophoretic separation on a 15% urea denaturing polyacrylamide gel electrophoresis (PAGE) gel. Small RNA regions with the 18- to 30-nt bands in the marker lane were excised and recovered. The 18- to 30-nt small RNAs were ligated to a 5'-adaptor and a 3'-adaptor. The adapter-ligated small RNAs were subsequently transcribed into cDNA by SuperScript II Reverse Transcriptase (Invitrogen, Waltham, MA, USA). PCR products were selected by agarose gel electrophoresis with target fragments 100–120 bp, and then purified by the QIAquick Gel Extraction Kit (QIAGEN, Valencia, CA, USA). The library was assessed for quality and quantity by checking the distribution of the fragment size using the Agilent 2100 bioanalyzer and by quantifying the library using qRT-PCR. The final ligation PCR products were sequenced using the BGISEQ-500 platform (BGI-Shenzhen, China).

miRNA sequencing data processing

The raw tags were processed using the following steps by removing low-quality tags, tags with 5 primer contaminants or poly A, tags without 3 primer or insertion, and tags shorter than 18 nt. After filtering, the clean tags were mapped to the reference genomes and other sRNA databases, including miRbase, siRNA, piRNA, and snoRNA with Bowtie2 (v2.2.5). MiRanda (v2.041), RNAhybrid (v2.1), and TargetScan (v5.0) were used to predict the target genes of miRNAs. The expression level of miRNA was calculated by counting the absolute number of molecules using unique molecular identifiers. Differential expression analysis was performed using the DEGseq (v1.4.5). Q value ≤ 0.001 and absolute value of Log2Ratio ≥ 1 were the default threshold to indicate the significance. To annotate gene functions, all target genes were aligned against the Kyoto Encyclopedia of Genes (KEGG) and Gene Ontology (GO) database. GO enrichment analysis (<http://www.geneontology.org/>) and KEGG enrichment analysis (<https://www.kegg.jp/>) of the target genes were performed using *phyper* in R software (v3.3.1). The *p* value was corrected using the Bonferroni method.

GO terms or KEGG terms were defined as significantly enriched terms only when corrected *p* value ≤ 0.05 .

mRNA library preparation and sequencing

Oligo(dT)-attached magnetic beads were used to purify mRNA. Purified mRNA was fragmented into small pieces with fragmentation buffer. First-strand cDNA was then generated using random hexamer-primed reverse transcription and followed by a second-strand cDNA synthesis. A-tailing mix and RNA index adapters were added by incubating to end repair. The cDNA fragments were amplified by PCR, and the products were purified by Ampure XP Beads. After dissolution in EB solution, the product was validated on the Agilent Technologies 2100 bioanalyzer. PCR products were heated, denatured, and circularized by the splint oligo sequence to obtain the final library. The single-strand circle DNA was formatted as the final library, which was then amplified with phi29 to make DNA nanoballs (DNBs) >300 copies per molecule. DNBs were loaded into the patterned nanoarray, and single end 50 base reads were generated on BGISEQ-500 platform (BGI-Shenzhen, China).

mRNA sequencing data processing

mRNA sequencing data were filtered with SOAPnuke (v1.5.2) by removing reads, which containing sequencing adapter, low-quality base ratio (base quality <5) $>20\%$, and unknown base ('N' base) ratio $>5\%$ [20]. Using HISAT2 (v2.0.4), the clean reads in FASTQ format were mapped to the reference genome. Then, Bowtie2 (v2.2.5) was applied to align the clean reads to the reference coding gene set, and then the expression level of gene was calculated by RSEM (v1.2.12). Differential expression analysis was performed using the DESeq2 (v1.4.5) with Q value ≤ 0.05 . GO and KEGG enrichment analyses of the annotated differentially expressed genes were performed by *phyper* based on Hypergeometric test. The significant levels of terms and pathways were corrected by Q value with a rigorous threshold (Q value ≤ 0.05) by Bonferroni method.

Validation by quantitative real-time polymerase chain reaction (qRT-PCR)

In order to verify the accuracy of transcriptome sequencing results, we randomly selected and confirmed the expressions of 5 mRNAs in ASTs exposed to two shapes (flake or rod) of γ -Al₂O₃-NPs by qRT-PCR. All primers are described in Additional file 1: Table S1. qRT-PCR was conducted with SYBR® Premix ExTaq™ II kit (TaKaRa Bio, Dalian, China) using a CFX96 Touch™ Detection System (Bio-Rad, CA, USA). Cycling conditions were 95 °C for 30 s, 44 cycles of 95 °C for 5 s, and 60 °C for 34 s. The expression of target genes was evaluated using

the $2^{-\Delta\Delta C_t}$ relative quantification method, normalized to *Actb* [21].

Statistical analysis

Statistical analysis was completed by using R software (v3.3.1). Statistical analyses of the expression levels of miRNAs and mRNAs were evaluated by multiple comparisons of Kruskal–Wallis rank sum test using *agricolae* package. After normalization, the expression levels of miRNAs and mRNAs were imported into R for principal components analysis (PCA) by using packages of *ropls* and *ggplot2*. Venn diagram and volcano plots were conducted by using the packages of *VennDiagram* and *ggplot2*, respectively. For the illustration of KEGG enrichment pathway analysis, bubble plots used *ggplot2*, *ggrepel* and *RColorBrewer* packages while heatmaps used *pheatmap*, *ggplot2* and *dplyr* packages. The interaction network analysis between the miRNAs and differentially expressed genes used Cytoscape software (v3.7.2) [22]. Q values (FDR) < 0.05 were considered as statistically significance for all data analysis.

Results

Analysis of small RNA and transcriptome sequencing

According to our previous research [14], although γ - Al_2O_3 -NPs of both shapes (flake or rod) caused a significant increase in cytotoxicity in a dose-dependent manner in rat ASTs exposed to 31.3, 62.5 and 125 $\mu\text{g}/\text{mL}$ for 72 h, the cytotoxic and apoptotic effects caused by nanorods were found to be significantly stronger than those of nanoflakes at the same dose, which might be due to the greater ROS levels of nanorod. In order to better understand the potential mechanisms of toxicities, the highest sublethal concentration of 125 $\mu\text{g}/\text{mL}$ of nanoflakes or nanorods were chosen in the present experiments.

The raw reads, clean reads, and other basic information of miRNAs and mRNAs, through small RNA sequencing and transcriptome analysis, are summarized in Table 1. For small RNA sequencing, 27.11, 26.13, and 26.49 million clean reads were acquired. miRDeep2 software further detected 659, 671, and 647 unique miRNAs in control, nanoflake, and nanorod groups, respectively. Among these, 578, 586, and 583 were known miRNAs, and 81, 85, and 64 were novel miRNAs in control, nanoflake, and nanorod groups, respectively (Table 1 and Additional file 1: Tables S2 and S3). For transcriptomes, after data filtering, a total of 21.74, 21.75, and 21.73 million clean reads were obtained in control, nanoflake, and nanorod groups, respectively.

Similarities and differences of the miRNA and mRNA profiles among three different groups were further assessed with PCA (Fig. 1A and B). Although both

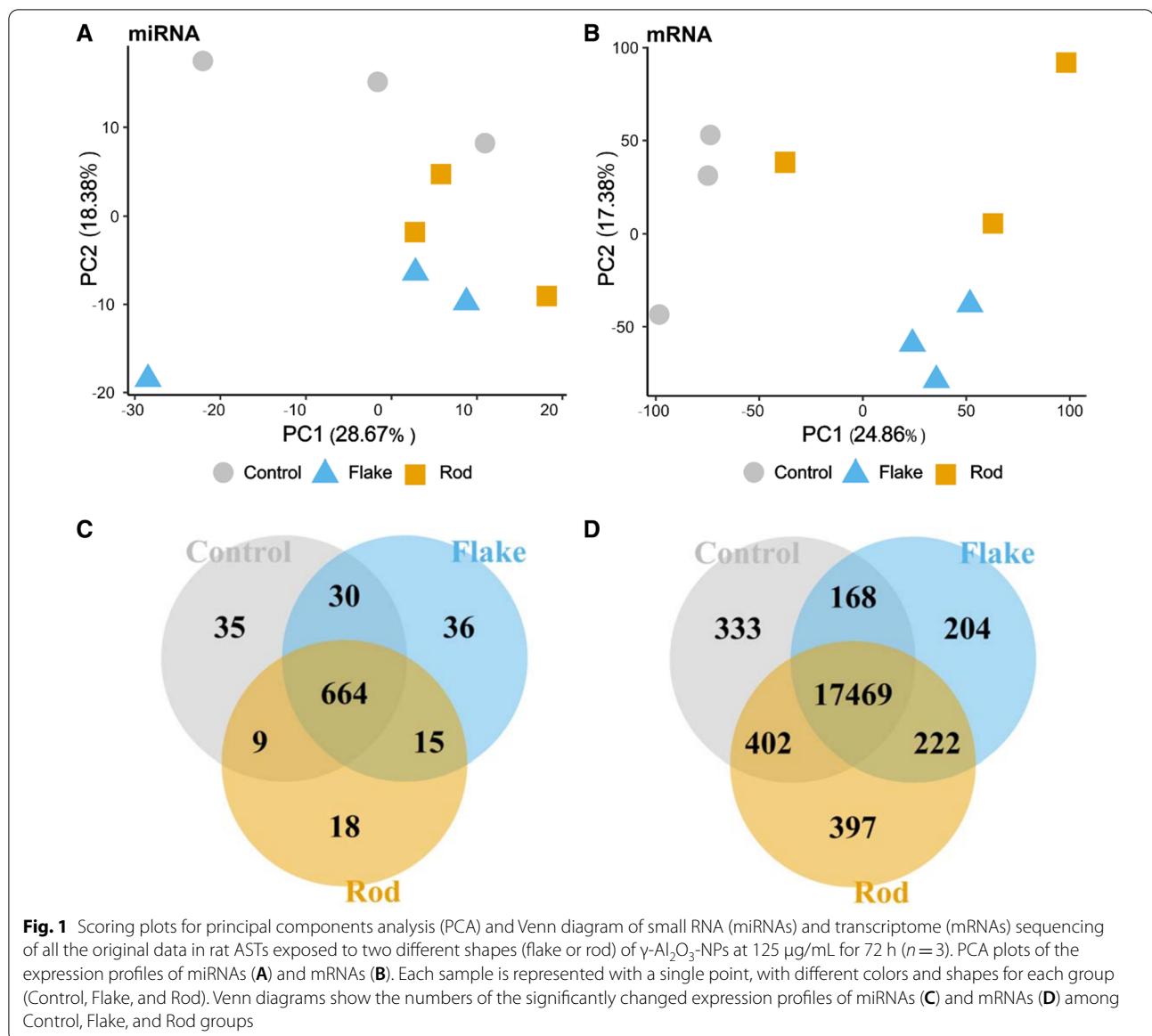
Table 1 Overview of small RNA (miRNA) with counts more than 10 and transcriptome (mRNA) sequencing in rat ASTs exposed to two different shapes (flake or rod) of γ - Al_2O_3 -NPs at 125 $\mu\text{g}/\text{mL}$ for 72 h ($n = 3$ for each group)

Category	Data type	Control	Flake	Rod
miRNA	Total raw reads (M)	29.32	28.59	28.95
	Total clean reads (M)	27.11	26.13	26.49
	Clean reads Q20 (%)	99.10	98.97	98.87
	Clean reads ratio (%)	92.44	91.40	91.53
	Total-miRNAs	659	671	647
	Known-miRNAs	578	586	583
	Novel-miRNAs	81	85	64
mRNA	Total raw reads (M)	21.80	21.78	21.77
	Total clean reads (M)	21.74	21.75	21.73
	Total clean bases (Gb)	1.09	1.09	1.09
	Clean reads Q30 (%)	90.61	91.15	91.23
	Clean reads ratio (%)	99.73	99.87	99.78

nanoflake and nanorod exposures drove separation from controls, largely along the PC 2 axis, the degree of separation of these two shapes was quite different, indicating that their toxicity mechanisms might be different.

Significantly changed miRNAs and mRNAs with nanoflake and nanorod exposures

Hierarchical cluster analyses of differentially expressed miRNAs and mRNAs in control, nanoflake, and nanorod groups are shown in Additional file 1: Figure S1. Among Venn diagrams of control vs nanoflakes, control vs nanorods, and nanoflakes vs nanorods, 15 miRNAs were significantly changed in both nanoflakes and nanorods, while 36 and 18 miRNAs were only found in nanoflake and nanorod exposures, respectively (Fig. 1C). Compared with control, volcano plots showed that 83 and 39 miRNAs were significantly up-regulated and down-regulated, respectively, in nanoflakes, while 44 and 72 miRNAs were significantly up-regulated and down-regulated, respectively, in nanorods (Fig. 2A and B). Therefore, some differences in miRNAs profiling were indeed found between nanoflakes and nanorods. Compared with the nanoflakes, there were 17 (12.59%) and 83 (61.48%) miRNAs significantly up-regulated and down-regulated in nanorods, respectively (Fig. 2C). 26 miRNAs were simultaneously increased in both nanoflake (23.21%) and nanorod (22.41%) groups, such as miR-151, miR-16, miR-24, miR-180, and miR-121, while 29 miRNAs were simultaneously decreased in both nanoflake (23.77%) and nanorod (25%) groups, such as miR-155, miR-35, miR-54, miR-65, and miR-164. Compared with the nanoflakes, 18 (15.52%) miRNAs (e.g., miR-46, miR-89, miR-178, miR-150, and miR-49) were specifically increased in the



nanorod group, while totally 43 (37.07%) miRNAs (e.g., miR-55, miR-105, miR-109, miR-11, and miR-120) were specifically decreased. 57 (46.72%) miRNAs (e.g., miR-70, miR-127, miR-61, miR-62, and miR-98) were specifically increased in the nanoflake group, while totally 10 (8.20%) miRNAs (e.g., miR-60, miR-113, miR-169, and miR-40) were specifically decreased.

Transcriptome analysis results also showed that the distinct gene expression profiles of γ - Al_2O_3 -NPs were

induced by the two different shapes. Compared with control, 222 mRNAs were significantly changed in both exposure groups, while 204 and 397 mRNAs were uniquely found in nanoflakes and nanorods groups, respectively (Fig. 1D). Similarly, volcano plots showed that 194 and 75 mRNAs were significantly up-regulated and down-regulated, respectively, in nanoflakes, while 130 and 50 mRNAs were significantly up-regulated and down-regulated, respectively, in nanorods (Fig. 2E and F).

(See figure on next page.)

Fig. 2 Volcano plots of miRNAs (A–C) and mRNAs (E–G) in rat ASTs exposed to two different shapes (flake or rod) of γ - Al_2O_3 -NPs at 125 $\mu\text{g}/\text{mL}$ for 72 h ($n = 3$). Each point represents a miRNA or mRNA, the expression level and negative logarithm of Q value (FDR) as the abscissa and ordinate, respectively. Pink and green dots represent the significantly up-regulated and down-regulated genes, respectively. Blue or gray dots represent miRNAs or mRNAs that were not differentially expressed. The total number of significantly differentially expressed genes is shown for miRNAs (D) and mRNAs (H). Group comparisons: Control vs Flake (A and E); Control vs Rod (B and F); Flake vs Rod (C and G)

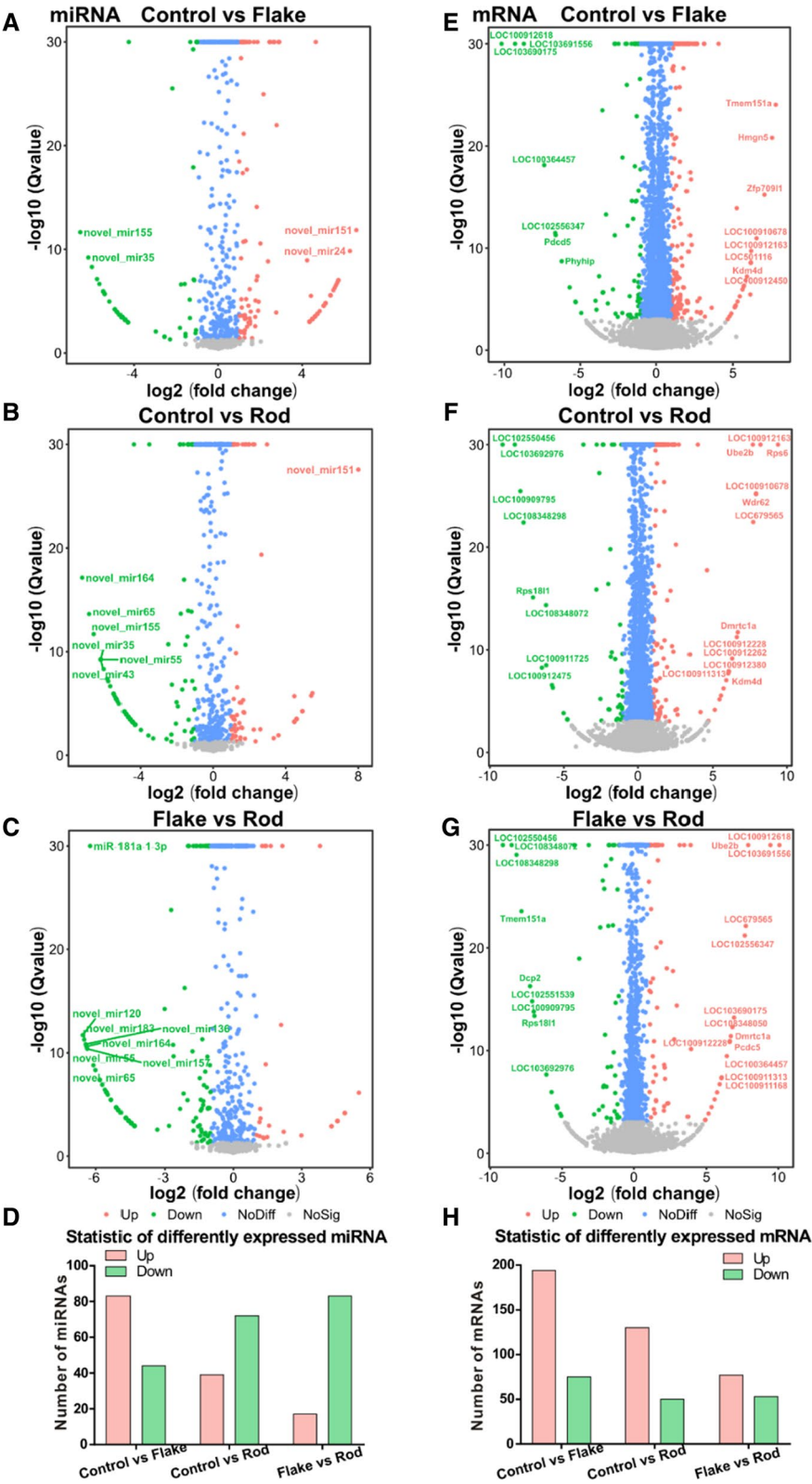


Fig. 2 (See legend on previous page.)

Compared with the nanoflakes, there were 77 (42.78%) and 53 (29.44%) mRNAs significantly up-regulated and down-regulated in nanorods, respectively (Fig. 2G and Additional file 1: Figure S2). 89 mRNAs were simultaneously increased in both nanoflakes (33.09%) and nanorods (49.44%), such as *Kdm4d*, *Wdr62*, and *Rps6*, while 16 mRNAs were simultaneously decreased in nanoflakes (5.95%) and nanorods (8.89%), such as *LOC103692976*, *LOC103690175*, and *LOC100912475*. Compared with nanoflakes, 41 (22.78%) mRNAs (e.g., *Dmrtc1a*, *Pou4f1*, and *Crkl*) were specifically increased in nanorods, while 34 (18.89%) mRNAs (e.g., *Fam98b*, *Pkhd1*, and *Rpl37*) were specifically decreased in total. 105 (39.03%) mRNAs (e.g., *Adora3*, *Sema3g*, and *Mmp28*) were specifically increased in nanoflakes, while 59 (21.93%) mRNAs (e.g., *Cftr*, *Akr1b8*, and *Cc2d2b*) were specifically decreased. In general, both shapes of γ -Al₂O₃-NPs significantly changed the profiling of miRNAs and mRNAs in rat ASTs, and the two shapes have different toxicity-related gene expression profiles.

Pathway enrichment analysis of nanoflakes and nanorods-modulated miRNAs and mRNAs

In order to explore the possible mechanisms of shape-dependent nanotoxicity, we performed the KEGG pathway enrichment analysis of the differentially expressed miRNAs and mRNAs in rat ASTs after nanoflake and nanorod exposures. KEGG pathway analysis revealed the linkages between our enriched data and cell signaling pathways [23]. Nanorods had a broader impact on the miRNA-induced pathways than that of nanoflakes. Compared with control, significantly changed miRNAs affected 97 signaling pathways after nanoflake exposure, while 141 signaling pathways were changed after nanorod exposure. There are 79 identical pathways both in nanoflakes (81.44%) and nanorods (56.03%) (e.g., NF- κ B (NF- κ B), mitogen-activated protein kinase (MAPK), and Rap1), and 18 (18.56%) and 62 (43.97%) specific pathways were observed in nanoflakes (e.g., Toll, pyruvate metabolism, and butanoate metabolism) and nanorods (e.g., phosphatidylinositol 3-kinase (PI3K)/Akt, adenosine monophosphate activated protein kinase (AMPK), TNF), respectively (Fig. 3A–C and Additional file 1: Figure S3 and Table S5).

Similar to miRNA pathway enrichment findings, nanorods had a greater impact on the mRNA-induced

pathways than that of nanoflakes. 13 and 23 signaling pathways were significantly changed by nanoflake and nanorod exposures, respectively. There are 6 identical pathways both in nanoflakes (46.16%) and nanorods (26.09%; e.g., Notch, sphingolipid metabolism, and ether lipid metabolism), 7 specific pathways in nanoflakes (53.84%; e.g., Toll, ABC transporters, and folate biosynthesis), and 17 specific pathways in nanorods (74.91%; e.g., ErbB, AMPK, cancer-related pathways) (Additional file 1: Table S4). Further, we found that both nanoflake and nanorod exposures could cause changes in environmental information processing-related signaling pathways (e.g., mTOR, Wnt, NF- κ B, Hippo, and calcium signaling pathways) (Fig. 3D, E, and Additional file 1: Figure S4). Compared with nanoflakes, the levels of lipolysis, apoptosis, and HIF-1 signaling pathways were significantly higher in nanorods (Fig. 3F). Furthermore, nanorod exposure was associated with the occurrence and development of multiple cancers, such as endometrial cancer, renal cell carcinoma, and non-small cell lung cancer (Fig. 3B and D). Altogether, KEGG results revealed that both shapes could activate inflammation and oncogenic signaling pathways, as well as change lipid metabolism in rat ASTs. Furthermore, nanorods have a more significant impact on these pathways compared to nanoflakes.

Interaction network of miRNAs and mRNAs

MiRNAs function post-transcriptionally by generally base-pairing with the 3'-untranslated regions of mRNAs to repress protein synthesis in animals, plants, and protozoa [24]. Therefore, we combined small RNA and transcriptome sequencing results to determine the transcriptional changes related to miRNA perturbations. Based on the interaction network of the significantly altered miRNAs and genes (mRNAs) constructed by Cytoscape, a unique interaction relationship between differentially expressed genes and miRNAs was observed between two different shapes (Fig. 4 and Additional file 1: Tables S6 and S7).

Compared with control, the expression of miRNAs (e.g., miR-760-5p, miR-383-3p, and miR-326-3p) were significantly up-regulated in nanoflakes. These miRNAs positively regulated the expressions of *Pde2a*, *Dpysl4*, *Elfn2*, *Tspan2* and *Col23a1* and negatively regulated the expressions of *Itga10* and *Gbp1* (Fig. 4A). Meanwhile,

(See figure on next page.)

Fig. 3 Bubble plots reveal the KEGG pathway enrichment analysis of significantly differentially expressed miRNAs (A–C) and mRNAs (D–F) in rat ASTs exposed to two different shapes (flake or rod) of γ -Al₂O₃-NPs at 125 μ g/mL for 72 h ($n = 3$). The vertical axis indicates the negative log₁₀ of Q value (FDR) of pathway enrichment analysis, and horizontal axis represents the number of genes annotated to the pathway, accounting for the proportion of the total number of genes. The size of the circle indicated the number of enriched miRNAs or genes. Group comparisons: Control vs Flake (A and D); Control vs Rod (B and E); Flake vs Rod (C and F)

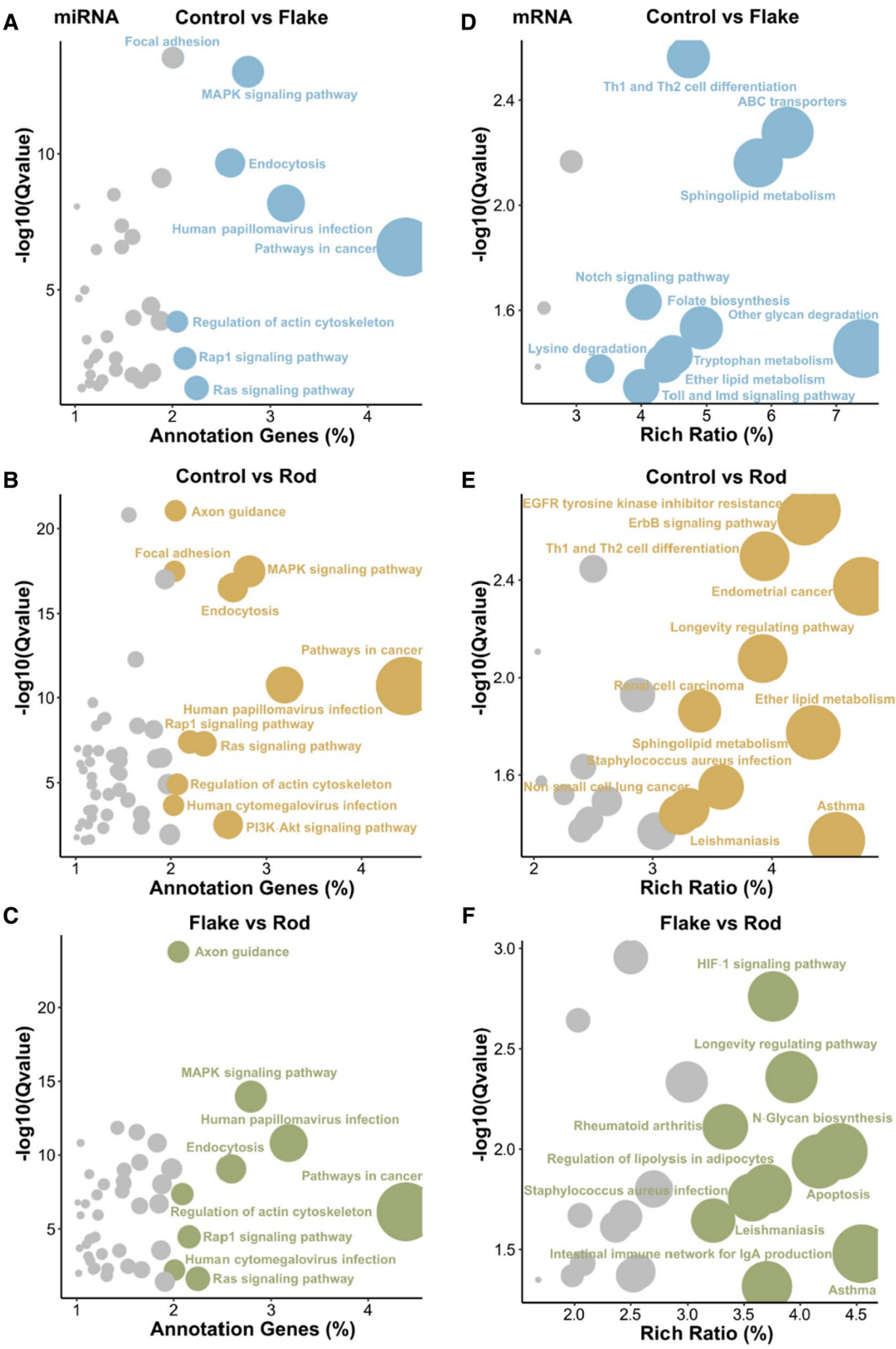
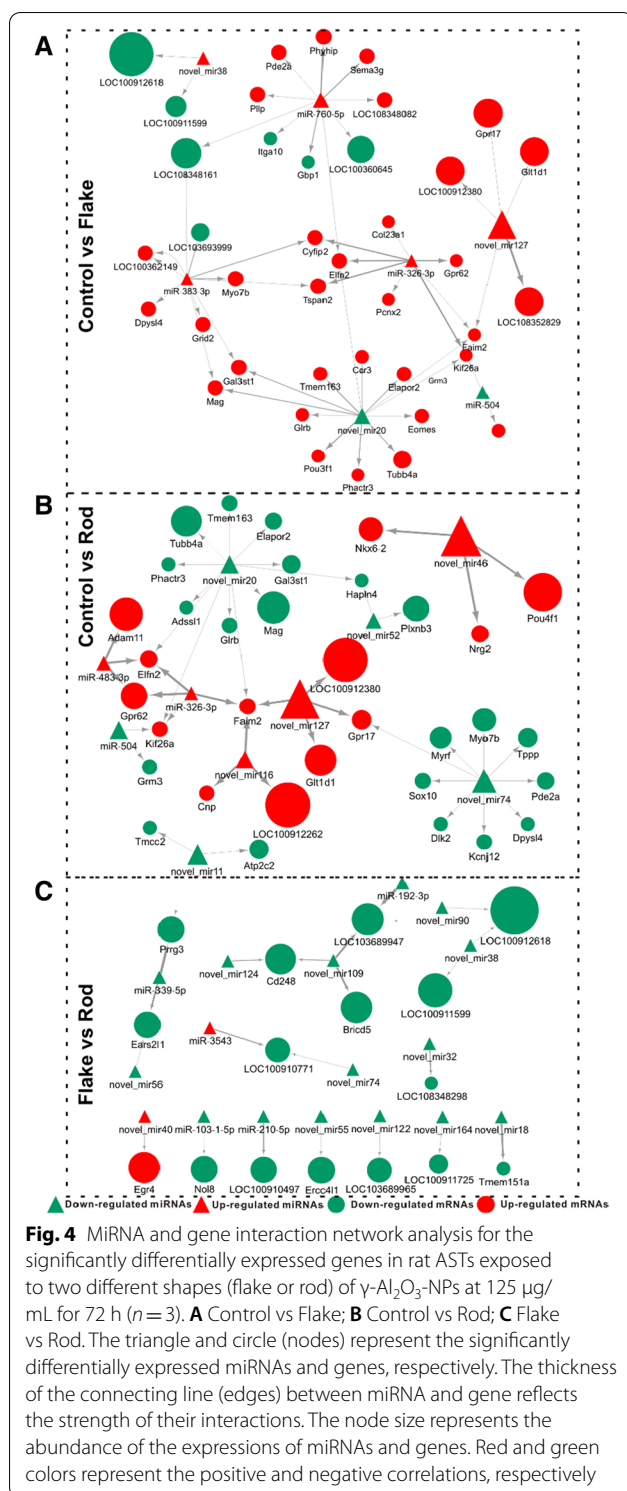


Fig. 3 (See legend on previous page.)



the expressions of known miRNAs (e.g., miR-504, miR-483-3p, and miR-383-3p) were significantly up-regulated in nanorods. A part of these miRNAs positively regulated the expressions of *Eln2*, *Gpr62* and *Faim2*, and some

miRNAs negatively regulated the expression of *Grm3* (Fig. 4B). Compared with nanorods, the expressions of miRNAs and genes, such as miR-55, miR-210-5p, *Nol8*, and *Prrg3*, were significantly down-regulated in nano-flakes (Fig. 4C). In addition, the significantly up-regulated or down-regulated miRNAs (e.g., miR-20, miR-74, and miR-127) were regarded as potential nanotoxicity-related genes.

Discussion

The adverse impact of Al_2O_3 -NPs on environment and human health has increased recently due to its wide application globally. They have been proven to exhibit neurotoxicity, genotoxicity, cytotoxicity, and developmental toxicity in animal and human cellular models [10, 25–27], mainly through the alternations in biomolecular pathways relevant to the accumulation of ROS, mitochondrial damages, immune disorders, and tissue injuries [4, 10–12]. As different shapes of NPs could interact and immobilize differently with plasma proteins, their corresponding toxicity profiles might be different in a shape-dependent manner. Although previous studies have demonstrated a size-dependent toxicity of γ - Al_2O_3 -NPs [28], comparative toxicological studies on differently shaped NPs (e.g., spheroidal and rod-like particles) have shown inconsistent results. In our previous study, a significant shape-dependent nanotoxicity was found [14]. Exposure to two different shapes of γ - Al_2O_3 -NPs (flake versus rod) could induce a significant cytotoxicity in rat ASTs in a dose-dependent manner, including significantly increased concentrations of inflammatory factors (IL-1 β , IL-2, and IL-6) and alternations in the metabolism of amino acids, lipids and purines, and pyrimidines. In the present study, to further clarify the role of morphology in distinct nanotoxicities, the significantly changed miRNAs and mRNAs were determined, and the toxic pathways induced by these two different shapes of γ - Al_2O_3 -NPs in rat ASTs were further elucidated and compared through small RNA and transcriptomics sequencings.

Here we found that both shapes of γ - Al_2O_3 -NPs induced a few consistent changes in miRNAs (e.g., miR-760-5p, miR-326-3p, and miR-35), mRNAs (e.g., *Eln2*, *Gpr62*, and *Kif26a*), and signaling pathways (e.g., MAPK, Rap1 and Ca^{2+} signaling). More specifically, both shapes simultaneously induced the up-regulation of miR-760-5p and miR-326-3p as well as the down-regulation of miR-35, suggesting their cytotoxic, neurotoxic, and carcinogenic potential. For example, the up-regulation of miR-760-5p has been linked to some neurotoxic symptoms (e.g., ataxic gait and head bobbing) in rats after 3,3'-iminodipropionitrile exposure [29]. Knockdown of miR-35 could result in an enhancement of MAPK signal transduction and a significant increase in *C.*

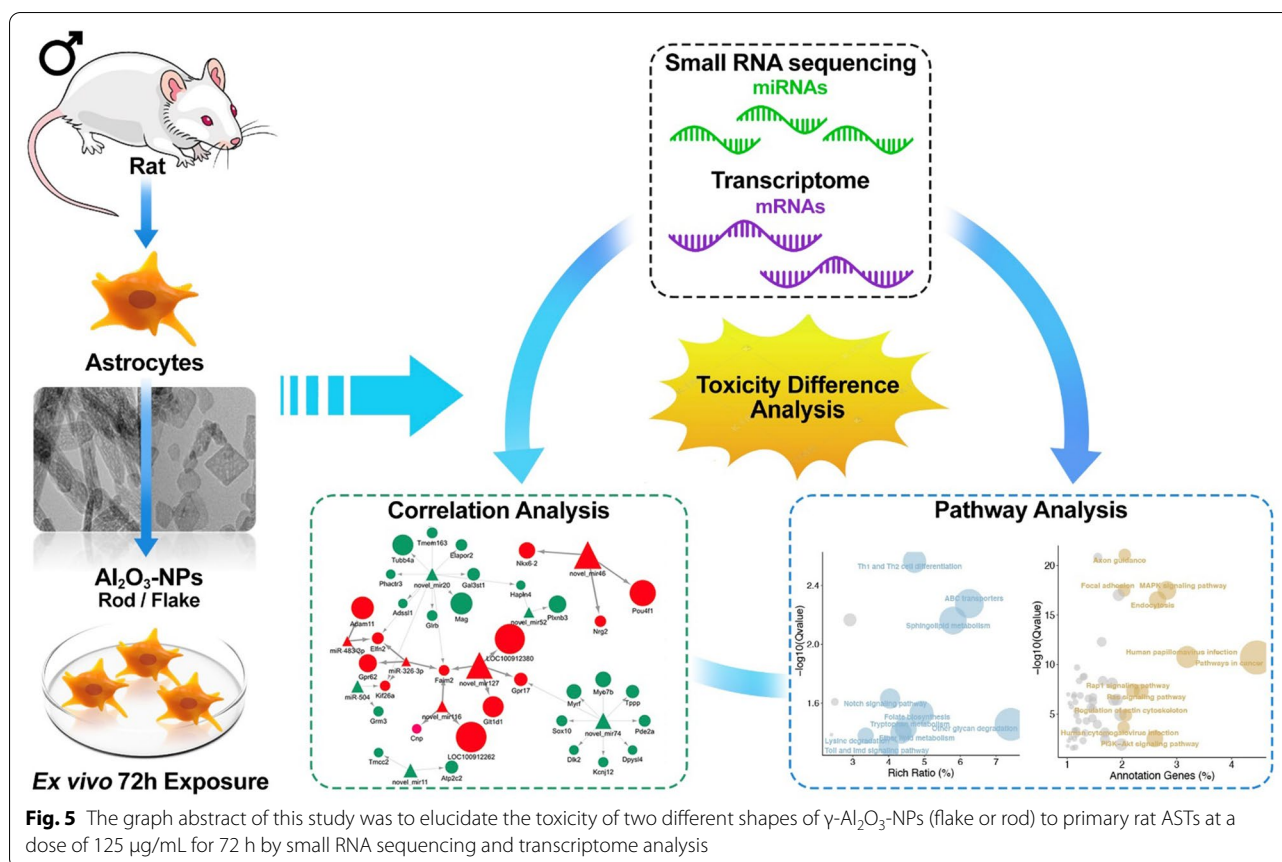
elegans germline death [30]. Interaction network analysis between the significantly altered miRNAs and mRNAs showed that both shapes up-regulated miR-326-3p and its downstream target gene *Elfn2*, which was essential for mGluRs signaling properties and brain function. *Elfn2* knockout mice showed a series of neuropsychiatric symptoms, including seizure susceptibility, hyperactivity disorder, and anxiety/compulsivity, suggesting that γ -Al₂O₃-NPs exposure might induce neurotoxicity through *Elfn2* [31]. Further, KEGG pathway analysis showed that the significantly changed miRNAs and mRNAs by both shapes were mainly enriched in MAPK, Rap1, and calcium signaling pathways. Intracellular Ca²⁺ signaling is fundamental to neuronal physiology and viability, and the disruption in Ca²⁺ could lead to a variety of disease processes, especially neurodegenerative diseases [32]. MAPK signaling pathway plays an important role in cell growth, development, differentiation, and apoptosis and contributes to the occurrence of neurodegenerative disorders [33]. In addition, Rap1 is mainly involved in the regulation of cell adhesion, which is over-activated in various tumors (e.g., breast cancers, prostate cancers, and melanoma), and plays a critical role in the migration, invasion, and metastasis of tumor cells [34, 35]. Lin et al. found that graphene oxide NPs exposure could trigger neuronal differentiation through Rap1–TRPC2–ERK1/2 pathway [36]. Both shapes of γ -Al₂O₃-NPs could induce changes in cell lipid metabolism, such as glycerol lipid metabolism, sphingolipid metabolism, and ether lipid metabolism. Sphingolipids are structural components of cell membrane, and the products of sphingolipids (e.g., ceramide, sphingosine-1-phosphate, and glucosylceramide) play an important role in apoptosis, proliferation, and drug resistance signaling [37]. It was thus suggested that γ -Al₂O₃-NPs might exert toxic effect by changing lipid metabolism. Altogether, these results show that there were certain consistent perturbations in miRNAs and mRNAs after two shapes of γ -Al₂O₃-NPs exposure, indicating that these changes were mediated through γ -Al₂O₃-NPs, irrespective of its morphology.

Moreover, morphology played an important role in the process of nanotoxicity. We previously observed that nanorods could induce a significantly higher apoptosis than that of nanoflakes, indicating its stronger toxicity [14]. In agreement with previous study, some differences in miRNA and mRNA perturbations between the two shapes were observed in this study. Compared to nanoflakes, nanorods could significantly up-regulate miR-55 and miR-150, suggesting that nanorods could have a greater cytotoxicity and carcinogenicity potential. For instance, Alizadeh et al. found that inhibition of miR-55 could increase the activity of Caspase-3 and induce apoptosis in Jurkat cells [1]. The level of miR-150

in patients with nasopharyngeal carcinoma was significantly increased and correlated with tumor distant metastasis and recurrence, and shortened the overall survival of patients [38]. Further, integration analysis showed that nanorods did not only cause the up-regulation of *Elfn*, but also up-regulate the expression of *Tspan2* and *Col23a1*, which were both the downstream target genes of miR-326-3p. *Tspan2* was positively correlated with the neuroinflammation and carcinogenesis, and *Tspan2* knockdown suppressed the metastasis to lung and liver, enabling prolonged survival [39]. Furthermore, compared with nanoflakes, the changes in signaling pathways were significantly induced by nanorods. Nanorods could especially activate PI3K/Akt, AMPK, and TNF signaling pathways. For example, the levels of neuroinflammatory cytokines (TNF-alpha, IL-6, and IL-1 β) were increased and memory and learning abilities were impaired in AlCl₃-induced AD rat models, which was consistent with the previous results that γ -Al₂O₃-NPs could induce an inflammatory response [40]. PI3K/Akt was closely related to cell apoptosis, the occurrence and development of tumors, and energy metabolism [41, 42]. Yang et al. found that PM_{2.5} exposure could cause the myocardial *ADRB2* hypermethylation and activate the PI3K/Akt pathway in AC16 cells, resulting in cardiomyocyte apoptosis as well as cardiac dysfunction [43]. In addition, compared with nanorods, nanoflakes could greatly activate the Toll and lmd signaling pathways, suggesting that nanoflakes could activate innate immune pathways. These studies demonstrate that nanorods might have stronger neurotoxicity, carcinogenicity, metabolic toxicity, and apoptotic ability, which might be mediated via morphology.

Conclusion

This is the first ex vivo study providing comprehensive evidence of distinct expression patterns regarding the changes of miRNAs and mRNAs in rat ASTs after two different types of γ -Al₂O₃-NP exposures (Fig. 5). Both shapes induced identical changes in miRNAs and mRNAs related to apoptosis, inflammatory pathways (e.g., NF- κ B), carcinogenic pathways (e.g., MAPK, p53, Notch, Rap1, and Ras), and cellular lipid metabolism (e.g., glycerolipid metabolism, sphingolipid, and ether lipid metabolism). However, the two different shapes also produced some distinct responses. It is evidenced that nanorods could specifically lead to the changes of PI3K/Akt, AMPK and TNF pathways, cell cycle, and cellular senescence, while nanoflakes specifically cause the changes of Toll and lmd signaling pathways, indicating that the previously observed higher toxicity with nanorods than nanoflakes, might be mediated through these differentially activated inflammatory and carcinogenic pathways and apoptosis. Further in vivo studies



are highly needed to verify these findings. The present study sheds light on the potential toxic mechanisms caused by the morphology of NPs, and demonstrates that multi-omics is a powerful approach to identify morphology-related toxicological signaling pathways, which could offer new intervention targets for the future treatment of NP-exposure related diseases.

Abbreviations

Al_2O_3 -NPs: Alumina nanoparticles; AMPK: Adenosine monophosphate activated protein kinase; ASTs: Astrocytes; *C. elegans*: *Caenorhabditis elegans*; DNBS: DNA nanoballs; HBE: Human bronchial epithelial; KEGG: Kyoto Encyclopedia of Genes; MAPK: Mitogen-activated protein kinase; miRNA: MicroRNA; NF- κ B: NF-kappa B; NPs: Nanoparticles; PBS: Phosphate buffered saline; PCA: Principal components analysis; qRT-PCR: Quantitative real-time polymerase chain reaction; ROS: Reactive oxygen.

Supplementary Information

The online version contains supplementary material available at <https://doi.org/10.1186/s12302-021-00540-9>.

Additional file 1. Additional Tables and figures.

Acknowledgements

Many thanks to Prof. Hongxing Dai and Xingtian Zhao from the Department of Chemistry and Chemical Engineering of Beijing University of Technology for their boundless helps in synthesizing and characterizing γ - Al_2O_3 -NPs.

Authors' contributions

YC: data curation, validation, and paper writing. LD: conceptualization, methodology, conducting experiments and paper writing. FD: investigation and data visualization. YC: data compilation and visualization. YF: literature search and data visualization. MZ: statistical analysis and interpretation. GQ: conceptualization and methodology. DS: reviewing and editing. KS: reviewing and editing. ST: funding acquisition, investigation, project administration, paper writing, and supervision. All authors read and approved the final manuscript.

Funding

This study was financially supported by the grants from the National Natural Science Foundation of China No. 21707132, Young Scholar Scientific Research Foundation of China CDC No. 2018A201, and Start-up Funding from NIEH, China CDC to Prof. Tang.

Availability of data and materials

The authors guarantee the authenticity of data and materials.

Declarations

Ethics approval and consent to participate

All animal experiments performed during this study were approved by the Institutional Animal Care and Use Committee (IACUC) of the Chinese Center for Disease Control and Prevention (China CDC No. 2016003). All the authors read and approved the final manuscript. The present findings have not been subjected to any peer and policy review from China CDC, and therefore does

not necessarily reflect the views of the China CDC and no official endorsement should be inferred.

Consent for publication

All authors approve this manuscript to be published in *Environmental Sciences Europe*.

Competing interests

The authors declare no conflicts of interest.

Author details

¹China CDC Key Laboratory of Environment and Population Health, National Institute of Environmental Health, Chinese Center for Disease Control and Prevention, No. 7 Panjiayuan Nanli, Chaoyang District, Beijing 100021, China. ²Center for Global Health, School of Public Health, Nanjing Medical University, Nanjing 211166, Jiangsu, China. ³Department of Preventive Medicine, Guangxi University of Chinese Medicine, Nanning 530200, Guangxi, China. ⁴Department of Chemical Engineering, Aristotle University of Thessaloniki, Thessaloniki, Greece. ⁵Department of Physiology, University of Alberta, Edmonton, Canada.

Received: 10 June 2021 Accepted: 5 August 2021

Published online: 16 August 2021

References

- Alizadeh S, Kaviani S, Soleimani M, Abroun S, Kashani-Khatib Z, Asgharzadeh A et al (2014) Mir-55 inhibition can reduce cell proliferation and induce apoptosis in Jurkat (Acute T cell Leukemia) cell line. *Iran J Ped Hematol Oncol* 4(4):141–150
- Keller AA, McFerran S, Lazareva A, Suh S (2013) Global life cycle releases of engineered nanomaterials. *J Nanopart Res* 15(6):1692
- Sadiq IM, Chowdhury B, Chandrasekaran N, Mukherjee A (2009) Antimicrobial sensitivity of *Escherichia coli* to alumina nanoparticles. *Nanomedicine* 5(3):282–286. <https://doi.org/10.1016/j.nano.2009.01.002>
- Li X, Zhang C, Zhang X, Wang S, Meng Q, Wu S et al (2016) An acetyl-L-carnitine switch on mitochondrial dysfunction and rescue in the metabolomics study on aluminum oxide nanoparticles. *Part Fibre Toxicol* 13:4. <https://doi.org/10.1186/s12989-016-0115-y>
- Townsend MC, Enterline PE, Sussman NB, Bonney TB, Rippey LL (1985) Pulmonary function in relation to total dust exposure at a bauxite refinery and alumina-based chemical products plant. *Am Rev Respir Dis* 132(6):1174–1180. <https://doi.org/10.1164/arrd.1985.132.6.1174>
- Yokel RA (2000) The toxicology of aluminum in the brain: a review. *Neurotoxicology* 21(5):813–828
- Balasubramanyam A, Sailaja N, Mahboob M, Rahman MF, Misra S, Hussain SM et al (2009) Evaluation of genotoxic effects of oral exposure to aluminum oxide nanomaterials in rat bone marrow. *Mutat Res* 676(1–2):41–47. <https://doi.org/10.1016/j.mrgentox.2009.03.004>
- Jalili P, Huet S, Lancelot R, Jarry G, Le Hegarat L, Nessler F et al (2020) Genotoxicity of aluminum and aluminum oxide nanomaterials in rats following oral exposure. *Nanomaterials*. <https://doi.org/10.3390/nano10020305>
- Li H, Huang T, Wang Y, Pan B, Zhang L, Zhang Q et al (2020) Toxicity of alumina nanoparticles in the immune system of mice. *Nanomedicine* 15(9):927–946. <https://doi.org/10.2217/nmm-2020-0009>
- Srikanth K, Mahajan A, Pereira E, Duarte AC, Venkateswara Rao J (2015) Aluminium oxide nanoparticles induced morphological changes, cytotoxicity and oxidative stress in Chinook salmon (CHSE-214) cells. *J Appl Toxicol* 35(10):1133–1140. <https://doi.org/10.1002/jat.3142>
- Park EJ, Lee GH, Shim JH, Cho MH, Lee BS, Kim YB et al (2015) Comparison of the toxicity of aluminum oxide nanorods with different aspect ratio. *Arch Toxicol* 89(10):1771–1782. <https://doi.org/10.1007/s00204-014-1332-5>
- Park EJ, Lee GH, Yoon C, Jeong U, Kim Y, Cho MH et al (2016) Biodistribution and toxicity of spherical aluminum oxide nanoparticles. *J Appl Toxicol* 36(3):424–433. <https://doi.org/10.1002/jat.3233>
- Huang LH, Sun XY, Ouyang JM (2019) Shape-dependent toxicity and mineralization of hydroxyapatite nanoparticles in A7R5 aortic smooth muscle cells. *Sci Rep* 9(1):18979. <https://doi.org/10.1038/s41598-019-55428-9>
- Dong L, Tang S, Deng F, Gong Y, Zhao K, Zhou J et al (2019) Shape-dependent toxicity of alumina nanoparticles in rat astrocytes. *Sci Total Environ* 690:158–166. <https://doi.org/10.1016/j.scitotenv.2019.06.532>
- Fröhlich E (2017) Role of omics techniques in the toxicity testing of nanoparticles. *J Nanobiotechnology* 15(1):84. <https://doi.org/10.1186/s12951-017-0320-3>
- Zhang S, Chu Q, Zhang Z, Xu Y, Mao X, Zhang M (2021) Responses of *Caenorhabditis elegans* to various surface modifications of alumina nanoparticles. *Environ Pollut* 271:116335. <https://doi.org/10.1016/j.envpol.2020.116335>
- Yun J, Yang H, Li X, Sun H, Xu J, Meng Q et al (2020) Up-regulation of miR-297 mediates aluminum oxide nanoparticle-induced lung inflammation through activation of Notch pathway. *Environ Pollut* 259:113839. <https://doi.org/10.1016/j.envpol.2019.113839>
- Burkley CE, Ashlock J, Winfrey WB, Zhang B (2012) Effects of aluminum oxide nanoparticles on the growth, development, and microRNA expression of tobacco (*Nicotiana tabacum*). *PLoS ONE* 7(5):e34783. <https://doi.org/10.1371/journal.pone.0034783>
- Reuther J, Roy A, Monzon FA (2019) Transcriptome Sequencing (RNA-Seq). *Genomic Applications in Pathology*. https://doi.org/10.1007/978-3-319-96830-8_4
- Chen Y, Chen Y, Shi C, Huang Z, Zhang Y, Li S et al (2018) SOAPnuke: a MapReduce acceleration-supported software for integrated quality control and preprocessing of high-throughput sequencing data. *Gigascience* 7(1):1–6. <https://doi.org/10.1093/gigascience/gix120>
- Chen YY, Wang WH, Che L, Lan Y, Zhang LY, Zhan DL et al (2020) BNIP3L-dependent mitophagy promotes HBx-induced cancer stemness of hepatocellular carcinoma cells via glycolysis metabolism reprogramming. *Cancers*. <https://doi.org/10.3390/cancers12030655>
- Shannon P, Markiel A, Ozier O, Baliga NS, Wang JT, Ramage D et al (2003) Cytoscape: a software environment for integrated models of biomolecular interaction networks. *Genome Res* 13(11):2498–2504. <https://doi.org/10.1101/gr.1239303>
- Kanehisa M, Sato Y, Furumichi M, Morishima K, Tanabe M (2019) New approach for understanding genome variations in KEGG. *Nucleic Acids Res* 47(D1):D590–d595. <https://doi.org/10.1093/nar/gky962>
- Fabian MR, Sonenberg N, Filipowicz W (2010) Regulation of mRNA translation and stability by microRNAs. *Annu Rev Biochem* 79:351–379. <https://doi.org/10.1146/annurev-biochem-060308-103103>
- Li Y, Yu S, Wu Q, Tang M, Wang D (2013) Transmissions of serotonin, dopamine, and glutamate are required for the formation of neurotoxicity from Al₂O₃-NPs in nematode *Caenorhabditis elegans*. *Nanotoxicology* 7(5):1004–1013. <https://doi.org/10.3109/17435390.2012.689884>
- Liu X, Tang J, Song B, Zhen M, Wang L, Giesy JP (2019) Exposure to Al₂O₃(3) nanoparticles facilitates conjugative transfer of antibiotic resistance genes from *Escherichia coli* to *Streptomyces*. *Nanotoxicology* 13(10):1422–1436. <https://doi.org/10.1080/17435390.2019.1669731>
- Zhu X, Zhu L, Duan Z, Qi R, Li Y, Lang Y (2008) Comparative toxicity of several metal oxide nanoparticle aqueous suspensions to Zebrafish (*Danio rerio*) early developmental stage. *J Environ Sci Health A Tox Hazard Subst Environ Eng* 43(3):278–284. <https://doi.org/10.1080/10934520701792779>
- Ates M, Demir V, Arslan Z, Daniels J, Farah IO, Bogatu C (2015) Evaluation of alpha and gamma aluminum oxide nanoparticle accumulation, toxicity, and depuration in *Artemia salina* larvae. *Environ Toxicol* 30(1):109–118. <https://doi.org/10.1002/tox.21917>
- Ogata K, Kushida M, Miyata K, Sumida K, Takeda S, Izawa T et al (2016) Alteration of microRNA expressions in the pons and medulla in rats after 3,3'-iminodipropionitrile administration. *J Toxicol Pathol* 29(4):229–236. <https://doi.org/10.1293/tox.2016-0019>
- Tran AT, Chapman EM, Flamand MN, Yu B, Krempel SJ, Duchaine TF et al (2019) MiR-35 buffers apoptosis thresholds in the *C. elegans* germline by antagonizing both MAPK and core apoptosis pathways. *Cell Death Differ* 26(12):2637–2651. <https://doi.org/10.1038/s41418-019-0325-6>

31. Dunn HA, Zucca S, Dao M, Orlandi C, Martemyanov KA (2019) ELFN2 is a postsynaptic cell adhesion molecule with essential roles in controlling group III mGluRs in the brain and neuropsychiatric behavior. *Mol Psychiatry* 24(12):1902–1919. <https://doi.org/10.1038/s41380-019-0512-3>
32. Demuro A, Parker I, Stutzmann GE (2010) Calcium signaling and amyloid toxicity in Alzheimer disease. *J Biol Chem* 285(17):12463–12468. <https://doi.org/10.1074/jbc.R109.080895>
33. Kim EK, Choi EJ (2015) Compromised MAPK signaling in human diseases: an update. *Arch Toxicol* 89(6):867–882. <https://doi.org/10.1007/s00204-015-1472-2>
34. Hattori M, Minato N (2003) Rap1 GTPase: functions, regulation, and malignancy. *J Biochem* 134(4):479–484. <https://doi.org/10.1093/jb/mvg180>
35. Ichikawa H, Itsumi M, Kajioka S, Maki T, Lee K, Tomita M et al (2018) Overexpression of exchange protein directly activated by cAMP-1 (EPAC1) attenuates bladder cancer cell migration. *Biochem Biophys Res Commun* 495(1):64–70. <https://doi.org/10.1016/j.bbrc.2017.10.142>
36. Lin L, Zhuang X, Huang R, Song S, Wang Z, Wang S et al (2020) Size-Dependent effects of suspended graphene oxide nanoparticles on the cellular fate of mouse neural stem cells. *Int J Nanomed* 15:1421–1435. <https://doi.org/10.2147/ijn.S225722>
37. Ogretmen B (2018) Sphingolipid metabolism in cancer signalling and therapy. *Nat Rev Cancer* 18(1):33–50. <https://doi.org/10.1038/nrc.2017.96>
38. Liu B, Tan Z, Jiang Y, Chen Y, Chen Y, Ling K (2018) Correlation between the expression of miR150 and FOXO4 and the local recurrence and metastasis of nasopharyngeal carcinoma after intensive radiotherapy. *J buon* 23(6):1671–1678
39. Otsubo C, Otomo R, Miyazaki M, Matsushima-Hibiya Y, Kohno T, Iwakawa R et al (2014) TSPAN2 is involved in cell invasion and motility during lung cancer progression. *Cell Rep* 7(2):527–538. <https://doi.org/10.1016/j.celrep.2014.03.027>
40. Yin S, Ran Q, Yang J, Zhao Y, Li C (2020) Nootropic effect of neferine on aluminium chloride-induced Alzheimer's disease in experimental models. *J Biochem Mol Toxicol* 34(2):e22429. <https://doi.org/10.1002/jbt.22429>
41. Kane LP, Weiss A (2003) The PI-3 kinase/Akt pathway and T cell activation: pleiotropic pathways downstream of PIP3. *Immunol Rev* 192:7–20. <https://doi.org/10.1034/j.1600-065x.2003.00008.x>
42. Ogawara Y, Kishishita S, Obata T, Isazawa Y, Suzuki T, Tanaka K et al (2002) Akt enhances Mdm2-mediated ubiquitination and degradation of p53. *J Biol Chem* 277(24):21843–21850. <https://doi.org/10.1074/jbc.M109745200>
43. Yang X, Zhao T, Feng L, Shi Y, Jiang J, Liang S et al (2019) PM(2.5)-induced ADRB2 hypermethylation contributed to cardiac dysfunction through cardiomyocytes apoptosis via PI3K/Akt pathway. *Environ Int* 127:601–614. <https://doi.org/10.1016/j.envint.2019.03.057>

Publisher's Note

Springer Nature remains neutral with regard to jurisdictional claims in published maps and institutional affiliations.

Submit your manuscript to a SpringerOpen[®] journal and benefit from:

- Convenient online submission
- Rigorous peer review
- Open access: articles freely available online
- High visibility within the field
- Retaining the copyright to your article

Submit your next manuscript at ► [springeropen.com](https://www.springeropen.com)